International Journal of Bifurcation and Chaos, Vol. 27, No. 10 (2017) 1750156 (19 pages)

DOI: 10.1142/S0218127417501565

Quantifying the Role of Folding in Nonautonomous Flows: The Unsteady Double-Gyre

K. G. D. Sulalitha Priyankara
Department of Mathematics,
The Clarkson Center for Complex Systems Science,
Clarkson University, 8 Clarkson Ave,
Potsdam, New York 13699-5815, USA
priyankg@clarkson.edu

Sanjeeva Balasuriya
School of Mathematical Sciences,
University of Adelaide, Adelaide, SA 5005, Australia
sanjeevabalasuriya@yahoo.com

Erik Bollt
Department of Mathematics,
Electrical and Computer Engineering,
The Clarkson Center for Complex Systems Science,
Clarkson University, 8 Clarkson Ave,
Potsdam, New York 13699-5815, USA
bolltem@clarkson.edu

Received February 24, 2017

We analyze chaos in the well-known nonautonomous Double-Gyre system. A key focus is on *folding*, which is possibly the less-studied aspect of the "stretching + folding = chaos" mantra of chaotic dynamics. Despite the Double-Gyre not having the classical homoclinic structure for the usage of the Smale–Birkhoff theorem to establish chaos, we use the concept of folding to prove the existence of an embedded horseshoe map. We also show how curvature of manifolds can be used to identify fold points in the Double-Gyre. This method is applicable to general nonautonomous flows in two dimensions, defined for either finite or infinite times.

Keywords: Chaos; horseshoe map; Double-Gyre; transverse intersection; curvature.

1. Introduction

A well-known mechanism through which chaos can arise in deterministic dynamical systems is by the combined effect of stretching and folding. Stretching will separate nearby points, while folding can abruptly bring together points which were initially far away. Various ways which quantify the stretching (most notably finite-time Lyapunov exponents) abound in the literature [Shadden *et al.*, 2005; Froyland & Padberg-Gehle, 2012; Balasuriya, 2016a; Tallapragada & Ross, 2013; Nevins & Kelley, 2016; Ma *et al.*, 2016]. *Folding*, however, is much less addressed. In this paper, we specifically focus on the concept of folding in two different ways. Firstly, it is used to prove that a highly-studied testbed for numerical methods — the Double-Gyre

[Shadden *et al.*, 2005] — is chaotic. While the fact that this system is chaotic is "known" anecdotally, it appears that a proof of this fact is not available, and we are able to provide it in this paper using the concept of folding in a specific way. Secondly, we propose a method for quantifying folding in general two-dimensional nonautonomous dynamical systems. This is through computing the curvature along distinguished one-dimensional curves of the system.

The presence of stretching and folding in a dynamical system leads to a range of properties usually associated with chaos (sensitivity to initial conditions, presence of countably many periodic orbits and uncountably many aperiodic ones, the presence of a dense orbit, etc). Smale's horseshoe map [Rössler, 1977; Holmes, 1986; Arrowsmith & Vivaldi, 1993; Chen, 2006; Alligood *et al.*, 1996] forms a paradigm for this mechanism, and in proving that this system is chaotic the basic strategy is to exploit the conjugacy of the map's action with shift dynamics on bi-infinite sequences [Alligood *et al.*, 1996; Namikawa & Hashimoto, 2004]. Thus, in proving that two-dimensional maps are chaotic, it is sufficient to establish the existence of horseshoe-like maps within them. One standard way in which this arises is through the presence of a transverse intersection between the stable and the unstable manifolds of a fixed point of the map; the Smale–Birkhoff theorem [Guckenheimer & Holmes, 1983; Holmes, 1990; Alligood *et al.*, 1996] provides a method for constructing the horseshoe map in that situation. The original theorem is for *homoclinic* situations; that is, there must be a transverse intersection between the stable and the unstable manifolds of the *same* fixed point of a discrete dynamical system. The basic intuition is that it is then possible to identify a quadrilateral piece of space near the intersection (call it A), which eventually gets mapped back on top of itself exactly like a horseshoe map. The homoclinic nature is crucial in this argument, since it enables A to get mapped "all the way round" since after it gets pulled out along the unstable manifold direction, it will then get pulled in along the stable manifold direction.

The Smale–Birkhoff theorem does not apply to the Double-Gyre flow [Shadden *et al.*, 2005], since it does not have a homoclinic structure. The Double-Gyre was initially proposed by Shadden *et al.* [2005] as a toy model for two adjacent oceanic gyres. It has since taken on a prominent role as a testbed in the development of a range of numerical diagnostics associated with transport and transport barriers [Allshouse & Peacock, 2015; Williams *et al.*, 2015; Pratt *et al.*, 2015; Balasuriya, 2016a; Sudharsan *et al.*, 2016; Rosi *et al.*, 2015; Garaboa-Paz & Perez-Munuzuri, 2015; Ma & Bollt, 2013; McIlhany & Wiggins, 2012; Mosovsky & Meiss, 2011; Brunton & Rowley, 2010; Lipinski & Mohseni, 2010; Duc & Siegmund, 2008; Tallapragada & Ross, 2013; Bollt *et al.*, 2012; Bollt, 2000; Bollt *et al.*, 2002; Froyland, 2013, etc.]. Numerics amply demonstrate that there is chaotic transport between the two gyres, which can each be thought of as a Lagrangian coherent structure [Haller, 2015; Kelley *et al.*, 2013; Haller & Yuan, 2000; Karrasch *et al.*, 2015; Onu *et al.*, 2015]. The field of Lagrangian coherent structures continues to attract tremendous interest, and there is in particular a multitude of diagnostic techniques that are either being refined or newly developed for the analysis of fluid transport associated with them. Well-established methods include finite-time Lyapunov exponent fields [Shadden *et al.*, 2005; He *et al.*, 2016; Huntley *et al.*, 2015; Nelson & Jacobs, 2015; Johnson & Meneveau, 2015; BozorgMagham & Ross, 2015; Branicki & Wiggins, 2010; Balasuriya & Ouellette, 2016], transfer (Perron–Frobenius) operator approaches [Froyland & Padberg-Gehle, 2009; Froyland *et al.*, 2007; Dellnitz & Junge, 2002; Froyland *et al.*, 2010], averages along trajectories [Wiggins & Mancho, 2014; Mancho *et al.*, 2013; Poje *et al.*, 1999; Mancho *et al.*, 2003; Mezic *et al.*, 2010] and curves of extremal attraction/repulsion [Blazevski & Haller, 2014; Teramoto *et al.*, 2013; Farazmand & Haller, 2013]. Other methods include clustering approaches [Hadjighasem *et al.*, 2016; Huntley *et al.*, 2015; Froyland & Padberg-Gehle, 2015], topological entropy [Balibrea & Snoha, 2003; Sattari *et al.*, 2016; Tumasz & Thiffeault, 2013], ergodic-theory related approaches [Budisic & Mezic, 2012] and curvature [Ma & Bollt, 2015; Ma *et al.*, 2016]. The latter approach is particularly relevant to the current paper, and will be revisited later. The main point, though, is that the Double-Gyre is often used to *test* these methods, sometimes against each other [Allshouse & Peacock, 2015]. In doing so, the "complicated" (i.e. chaotic) nature of the Double-Gyre is taken as given. However, there is as yet no proof that it is actually chaotic!

From the theoretical perspective, the impediment to using the Smale–Birkhoff theorem is that the entity separating the two gyres is not homoclinic, but rather *heteroclinic*. That is, it is associated with the stable manifold of a fixed point (of a relevant Poincaré map), and the unstable manifold of a *different* fixed point, intersecting. The standard horseshoe construction fails in this situation. An approach might be to appeal to an extension of the Smale–Birkhoff theorem due to Bertozzi [1988], in which she considers a "heteroclinic cycle" in which intersection patterns between stable/unstable manifold structures of a collection of fixed points form a cycle. Under *generic* conditions, it is then shown that a horseshoe construction can be made in this situation as well [Bertozzi, 1988]; effectively, the region A gets mapped around, going near each fixed point, and eventually returning to form a horseshoe-like set falling on top of A. Unfortunately, the Double-Gyre does *not* fall into this generic situation. While there is a heteroclinic cycle geometry in the Double-Gyre, only one of the connections between fixed points possesses the generic transverse intersection pattern. All other connections are situations in which a stable manifold *coincides* with an unstable manifold, and thus the heteroclinic extension [Bertozzi, 1988] to the Smale–Birkhoff theorem is inapplicable.

Given the importance of the Double-Gyre as a testbed, and the implicit agreement that it *is* chaotic, an actual *proof* of its chaotic nature would seem important. We provide exactly that in Sec. 2. We first develop analytical approximations to the stable and unstable manifolds. These are then used to identify "fold points" which are the basis for a horseshoe construction, leading to Theorem 5 in which we establish the chaotic nature of the Double-Gyre.

A main ingredient leading to chaos appearing in the Double-Gyre is the fact that the stable and unstable manifolds *fold*. We address this issue in a complementary fashion in Sec. 3. Here, we are inspired by recent work on using *curvature* in Lagrangian coherent structure analysis [Ma & Bollt, 2014]. In the current context, though, the argument is simple: if stable/unstable manifolds fold, then the curvature at those fold points must get anomalously large. Using the Double-Gyre as a testbed, we both numerically and theoretically track such points of large curvature. We establish numerically that the fold points do indeed possess the behavior established in our proof of chaos in the Double-Gyre. Using the curvature in this way can be done for general two-dimensional nonautonomous flows. The Double-Gyre is time-periodic, which allows for thinking of the dynamical system either in continuous time, or in discrete time (in relation to a Poincaré map). However, it is possible to use the curvature in nonautonomous systems with any time-dependence, by thinking of the stable and unstable manifolds as being attached to hyperbolic trajectories [Ju *et al.*, 2003; Muller-Karger *et al.*, 2000; Vleck, 1994] rather than fixed points. Moreover, using curvature in this way can also be done for specialized curves arising from using any diagnostic procedure in *finite-time* flows.

2. Horseshoe Map Chaos in the Double-Gyre Flow

The Double-Gyre flow was initially introduced by Shadden *et al.* [2005], and has since been studied extensively as a canonical example of complicated transport in nonautonomous flows [Allshouse & Peacock, 2015; Williams *et al.*, 2015; Pratt *et al.*, 2015; Balasuriya, 2016a; Sudharsan *et al.*, 2016; Rosi *et al.*, 2015; Garaboa-Paz & Perez-Munuzuri, 2015; Ma & Bollt, 2013; McIlhany & Wiggins, 2012; Mosovsky & Meiss, 2011; Brunton & Rowley, 2010; Lipinski & Mohseni, 2010; Duc & Siegmund, 2008, etc.]. Its flow is given by

$$\left.\begin{aligned} \dot{x}_1 &= -\pi A \sin[\pi\phi(x_1,t)]\cos[\pi x_2] \\ \dot{x}_2 &= \pi A \cos[\pi\phi(x_1,t)]\sin[\pi x_2]\frac{\partial\phi}{\partial x_1}(x_1,t) \end{aligned}\right\}, \tag{1}$$

in which $A > 0$ and $0 < \varepsilon \ll 1$, and

$$\phi(x_1,t) := \varepsilon\sin(\omega t)x_1^2 + (1 - 2\varepsilon\sin(\omega t))x_1.$$

This is usually viewed in the spatial domain $\Omega := [0,2]\times[0,1]$, and when $\varepsilon = 0$ possesses two counter-rotating gyres: one in $(0,1)\times(0,1)$ and the other in $(1,2)\times(0,1)$. This is a steady situation in which the gyres are separated by a heteroclinic manifold $x_1 = 1$, which is the stable manifold of $(1,0)$ and the unstable manifold of $(1,1)$. This manifold can be expressed parametrically by

$$\left.\begin{aligned} \overline{x}_1(t) &= 1, \\ \overline{x}_2(t) &= \frac{2}{\pi}\cot^{-1} e^{\pi^2 A t}; \end{aligned}\right. \quad t \in \mathbb{R}, \tag{2}$$

which is an exact solution to (1), with t representing time, when $\varepsilon = 0$. Here, $t = 0$ corresponds to $x_2 = 1/2$, and $\bar{x}_2(t) \to 1$ when $t \to -\infty$ and $\bar{x}_2(t) \to 0$ when $t \to \infty$.

When $\varepsilon \neq 0$, the flow (1) is nonautonomous. In this case of the "classical" Double-Gyre, it is time-periodic as well (for an analysis similar to what is to be presented for the *aperiodic* Double-Gyre, see [Balasuriya, 2016a]). Despite the nonautonomous nature, the lines $x_1 = 0$, $x_1 = 2$, $x_2 = 0$ and $x_2 = 1$ (i.e. the boundary of Ω) remain invariant. Thus, there is no possibility of chaotic motion being created in the system by the mechanism reported by Bertozzi [1988], which requires the heteroclinic network to break apart all the way around. However — as is well-known anecdotally and numerically though a proof does not seem to appear in the literature yet — the heteroclinic manifold which separates the two gyres, *does* break apart such that transverse intersections are created. The proof is straightforward.

Theorem 1 [Heteroclinic Intersections]. *There exists ε_0 such that for $|\varepsilon| \in (0, \varepsilon_0)$, at any time t, the stable and unstable manifolds adjacent to $x_1 = 1$ intersect each other transversely an infinite number of times.*

Proof. See Appendix A. ■

Despite perhaps conventional belief, Theorem 1 does not in and of itself prove the presence of *chaos* in the Double-Gyre. The original Smale–Birkhoff theorem [Guckenheimer & Holmes, 1983; Holmes, 1990; Alligood *et al.*, 1996] can only guarantee chaos, in the sense of symbolic dynamics, for *homoclinic* tangles. If the heteroclinics on the outer boundaries of Ω also exhibited heteroclinic tangling, then the results of Bertozzi [1988] can help extend this result. This is because fluid would travel from one heteroclinic tangle to the next, and so on, until arriving back again in the region of the initial tangle. It can be shown [Bertozzi, 1988] that dynamics similar to Smale's horseshoe map [Guckenheimer & Holmes, 1983; Holmes, 1990; Alligood *et al.*, 1996] ensues, and a continual repetition of this process can be proven to produce chaotic dynamics. However, in this case the heteroclinic manifolds on the boundary of Ω in the Double-Gyre *do not break apart*. Indeed, (1) was proposed [Shadden *et al.*, 2005] to preserve these boundaries, in order for it to be a model for an oceanic Double-Gyre enclosed by land. Therefore, additional work is needed to establish how *chaotic* transport occurs in the Double-Gyre due to the heteroclinic tangle adjacent to $x_1 = 1$.

The crux to the argument is the fact that the stable and unstable manifolds in the heteroclinic tangle have *folds* in them. We will show that fluid adjacent to such folds gets transported around the gyres and back again into the heteroclinic tangle region. In doing so, we will need analytical approximations for the stable and unstable manifolds, and the hyperbolic trajectories to which they are attached, for small $|\varepsilon|$. In the following, we think of these entities as *nonautonomous* ones, i.e. not necessarily in terms of a Poincaré map. From this viewpoint, a hyperbolic trajectory is defined in terms of exponential dichotomy conditions [Coppel, 1978; Battelli & Lazzari, 1986; Palmer, 1984; Balasuriya, 2016a, 2016b], and its local stable manifold is associated with the projection operator of the exponential dichotomy. The global stable manifold is of course the continuation of this. All these entities are therefore parametrized by time $t \in \mathbb{R}$. The time-periodicity property of the Double-Gyre will allow for identification of these nonautonomous entities equivalently in terms of a Poincaré map P_t which takes the flow from time t to $t + 2\pi/\omega$; the hyperbolic trajectory location would be a hyperbolic fixed point of P_t and the nonautonomous stable manifold will coincide with the stable manifold (with respect to P_t) of this hyperbolic fixed point. The advantage of the nonautomous viewpoint is that the variation with t is retained, whereas if considering a Poincaré map P_t then it is necessary to think of $t \in [0, 2\pi/\omega)$. Thus, there is in actuality a *family* of Poincaré maps. We will go back and forth between these continuous-time and discrete-time viewpoints, as needed.

Using the continuous-time approach, the hyperbolic trajectory and (a part of) its stable manifold can be approximated by the following theorem.

Theorem 2 [Stable Manifold]. *Let $P \in \mathbb{R}$ be given. Then, there exists ε_0 such that for $|\varepsilon| \in (0, \varepsilon_0)$, the saddle point at $(1, 0)$ when $\varepsilon = 0$, perturbs to a time-varying hyperbolic trajectory $\mathbf{x}_h^s(t) = (x_h^s(t), 0)$ given by*

$$x_h^s(t) = 1 + \varepsilon \cos\theta \sin(\omega t + \theta) + \mathcal{O}(\varepsilon^2);$$
$$\theta := \tan^{-1} \frac{\omega}{A\pi^2}. \tag{3}$$

Moreover, the stable manifold emanating from $\mathbf{x}_h^s(t)$ *at a time* t *can be approximated in the vicinity of* $x_1 = 1$ *in the parametric form*

$$\left.\begin{aligned} x_1^s(p,t) &= 1 + \varepsilon \frac{\pi^2 A}{\operatorname{sech}(\pi^2 A p)} \\ &\quad \times \int_p^\infty \tanh(\pi^2 A\tau)\operatorname{sech}(\pi^2 A \tau) \\ &\quad \times \sin[\omega(\tau + t - p)]\mathrm{d}\tau + \mathcal{O}(\varepsilon^2) \\ x_2^s(p,t) &= \frac{2}{\pi}\cot^{-1} e^{\pi^2 A p} \end{aligned}\right\}, \tag{4}$$

for $p \in [P, \infty)$, *and moreover if its reciprocal slope at* $\mathbf{x}_h^s(t)$, *is* $\theta_s(t)$, *then there exists* K_s *such that* $|\theta_s(t)| \le \varepsilon^2 K_s$ *for* $(t, \varepsilon) \in \mathbb{R} \times [0, \varepsilon_0)$.

Proof. See Appendix B. ■

An alternative expression for the leading-order stable manifold can be obtained by eliminating the parameter p from (4). Since

$$p = \frac{1}{\pi^2 A}\ln\left(\cot\frac{\pi x_2}{2}\right)$$

the stable manifold's leading-order term at each time t can be expressed as a graph from x_2 to x_1. Now, a similar theorem holds for the unstable manifold.

Theorem 3 [Unstable Manifold]. *Let* $P \in \mathbb{R}$ *be given. Then, there exists* ε_0 *such that for* $|\varepsilon| \in (0, \varepsilon_0)$, *the saddle point at* $(1,1)$ *when* $\varepsilon = 0$, *perturbs to a time-varying hyperbolic trajectory* $\mathbf{x}_h^u(t) = (x_h^u(t), 1)$, *given by*

$$\begin{aligned} x_h^u(t) &= 1 + \varepsilon\cos\theta\sin(\omega t - \theta) + \mathcal{O}(\varepsilon^2); \\ \theta &:= \tan^{-1}\frac{\omega}{A\pi^2}. \end{aligned} \tag{5}$$

Moreover, the unstable manifold emanating from $\mathbf{x}_h^u(t)$ *at a time* t *can be approximated in the vicinity of* $x_1 = 1$ *in the parametric form*

$$\left.\begin{aligned} x_1^u(p,t) &= 1 - \varepsilon \frac{\pi^2 A}{\operatorname{sech}(\pi^2 A p)} \\ &\quad \times \int_{-\infty}^p \tanh(\pi^2 A\tau)\operatorname{sech}(\pi^2 A \tau) \\ &\quad \times \sin[\omega(\tau + t - p)]\mathrm{d}\tau + \mathcal{O}(\varepsilon^2) \\ x_2^u(p,t) &= \frac{2}{\pi}\cot^{-1} e^{\pi^2 A p} \end{aligned}\right\}, \tag{6}$$

for $p \in (-\infty, P]$, *and moreover if its reciprocal slope at* $\mathbf{x}_h^u(t)$ *is* $\theta_u(t)$, *then there exists* K_u *such that* $|\theta_u(t)| \le \varepsilon^2 K_u$ *for* $(t, \varepsilon) \in \mathbb{R} \times [0, \varepsilon_0)$.

Proof. The proof is similar to that of Theorem 2, and will be skipped. ■

By taking the limit as $p \to \infty$ of the p-derivative of the expression (4), it is possible to show that the direction of emanation of the stable manifold remains vertical to $\mathcal{O}(\varepsilon)$. The same is true for the unstable manifold; these observations are a special case of the manifold emanation theory developed in [Balasuriya, 2016b]. Now, we have already established that the unstable and stable manifolds intersect infinitely often. Using the expressions in Theorems 2 and 3, the nature of this intersection pattern, and the lobes created as a result of these intersections, can be determined. We show the intersection pattern at a particular time instance in Fig. 1, which was produced with the analytical approximation obtained above, but the computation of the unstable manifold was stopped after a point. The unstable manifold can be represented as $x_1 = x_1(x_2)$ for $p < P_m$ (where P_m is an unspecified value), because for $p \to -\infty$, the unstable manifold approaches the hyperbolic trajectory $\mathbf{x}_h^u$, from which the unstable manifold emanates in a well-defined manner. In this region, we shall refer to the unstable manifold as the *primary* unstable manifold, for which (6) gives a good approximation for small enough $|\varepsilon|$. Larger p-values correspond to approaching $x_2 = 0$, and here, the unstable manifold will criss-cross the stable manifold infinitely often between the displayed ending and $x_2 = 0$. The stable manifold near $x_2 = 0$ is nearly a straight line emanating upwards from the point $\mathbf{x}_h^s(t)$. However, the intersection points with the criss-crossing unstable manifold must accumulate to $\mathbf{x}_h^s(t)$, forcing the corresponding lobes to get elongated in the $\pm x_1$-directions in order to maintain incompressibility. Thus, the unstable manifold in this region will be influenced by global effects, and hence the expression (6) becomes illegitimate. It may not be possible to represent the unstable manifold in the form $x_1 = x_1(x_2)$ in this *nonprimary* region. We are able to prove that this is indeed the case, while highlighting a particular behavior.

Theorem 4 [Fold Re-entrenchment]. *Let* $t \in \mathbb{R}$, *and suppose* $\delta > 0$ *is given. Define* N_δ *to be the one-sided neighborhood of the primary unstable manifold of width* δ, *near the hyperbolic trajectory location*

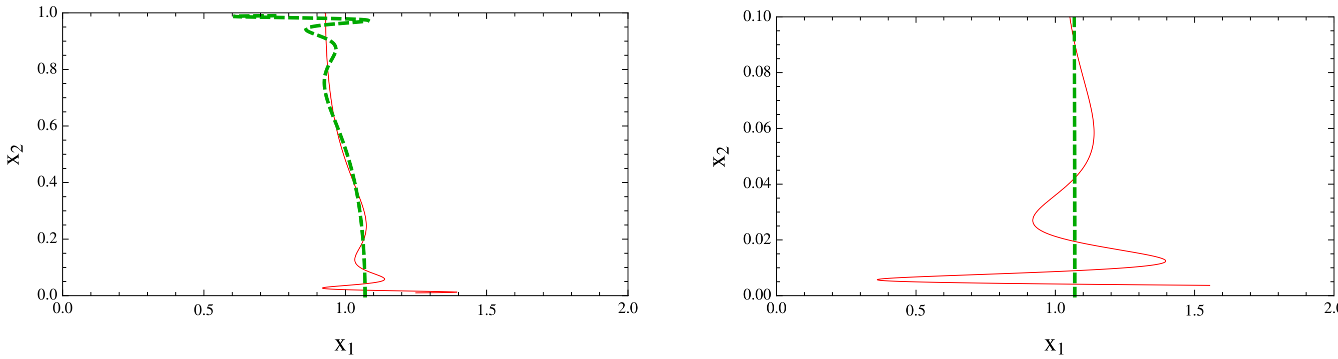

(a) (b)

Fig. 1. Intersection pattern of stable (dashed green) and unstable (solid red) manifolds predicted by Theorems 2 and 3, obtained using the $\mathcal{O}(\varepsilon)$-formulæ at $t = 0$ with $\varepsilon = 0.3$, $A = 1$ and $\omega = 40$: (a) in the full domain and (b) zoomed in close to $x_2 = 0$.

$\mathbf{x}_h^u(t) = (x_h^u(t), 1)$, as shown in Fig. 2. Then, there exists ε_0 such that for any $\varepsilon \in (0, \varepsilon_0)$, the unstable manifold emanating from $\mathbf{x}_h^u(t)$ will wrap around the gyre and re-enter N_δ, forming a fold in the sense that there is a region within this neighborhood such that a horizontal line will intersect the unstable manifold at least twice.

Proof. See Appendix C. ■

The geometry associated with Theorem 4 is shown in Fig. 2. There is a heteroclinic network (shown in blue) connecting the nonautonomous

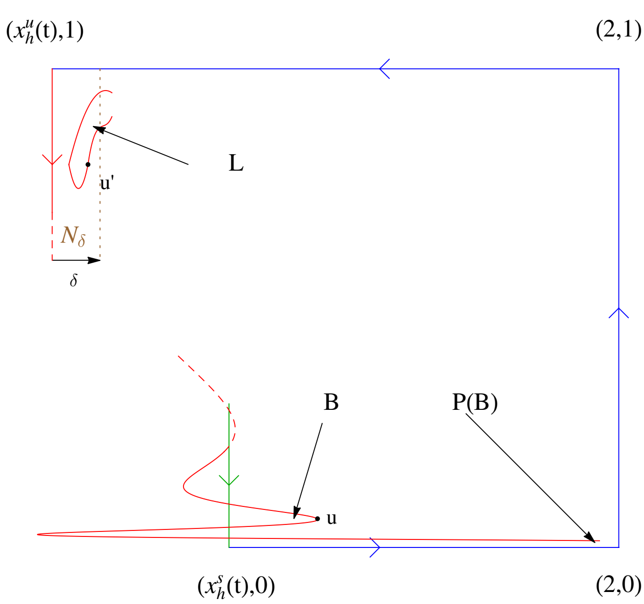

Fig. 2. The geometry around the right gyre which ensures that the unstable manifold returns to within δ of itself after wrapping around the boundary of Ω, as described in Theorem 4 and Appendix C.

hyperbolic trajectories $\mathbf{x}_h^s(t)$ and $\mathbf{x}_h^u(t)$ along the outer boundaries of Ω. This figure only shows the network around the right gyre, but there is a similar one around the left. We note that this is a degenerate situation in that the heteroclinic network does *not* break apart in a transverse way. The parts along the boundary of Ω simply persist as straight lines. This is to be contrasted with the results of Bertozzi [1988] that *generically*, heteroclinic networks which exist for $\varepsilon = 0$ break apart through transverse intersections along each heteroclinic segment. The Double-Gyre does not follow this, because the nature of the flow is such that the boundary of Ω is forced to remain invariant and regular. Therefore, Bertozzi's method for proving existence of a chaotic Smale horseshoe and chaotic transport in a heteroclinic tangle does not apply for the Double-Gyre. This is because we have had to establish Theorem 4 as a first step in our alternate proof of chaos.

The main point of Theorem 4 is that an unstable manifold segment L with a fold in it can be found in any arbitrarily small strip of width δ near the primary part of the unstable manifold emanating from $(x_h^u(t), 1)$. The precise shape of this unstable manifold segment is unknown; for example, it may possess many folds. However, Theorem 4 ensures that there will be *at least one* fold, in the sense that on the two sides of such a fold point, the unstable manifold has a larger x_2 value than at the fold point. We note that there is no claim that fold points are mapped to fold points. That is, it is not necessarily true that the point labeled u in Fig. 2 will eventually flow to the leading fold in L. Its image, u', need not be a fold point at all.

Now with the re-entrenchment theorem, we are ready to show that the Double-Gyre flow has an embedded horseshoe map. The standard Smale horseshoe map is well known [Robinson, 1999; Bollt & Santitissadeekorn, 2013] to be the map of rectangle, $T_\gamma : R \to R$ across itself, which in briefest terms, implies the standard package of results corresponding to fully developed chaos. Here, our "rectangle" will be slightly different.

Theorem 5 [Horseshoe Map]. *The Double-Gyre system has an embedded horseshoe, near the point* $(1, 1)$*. As such, the dynamics of the system is equivalent to a shift-map on a restricted subset, and there is fully developed chaos, at least on this subset.*

Proof. See Fig. 3. Near the point, $(1, 1)$, the unstable manifold shown has been established above. A set A, shown by the red boundaries, will be constructed in the re-entrechment region guaranteed by Theorem 4. A "vertical" line, parallel to the emergent unstable manifold, comprises its left boundary. We next note that there is an infinite number of re-entrenching lobes accumulating to the primary unstable manifold. Thus, the curves associated with these lobes, while entering the region "horizontally," will become "vertical" in approaching the unstable manifold. This enables the drawing of the "top" boundary of A as a curve which passes through the hyperbolic trajectory but is then normal to each of the curve segments comprising the re-entrenching lobes; see Fig. 3. The "bottom" boundary can also be constructed using the same orthogonality idea. Finally, the "right" boundary of A is formed by drawing a curve which does not intersect any lobe. Having constructed A, choose n to be large enough such that when applying the strobing Poincaré map P n-times to A, part of the set A will stretch along the unstable manifold *and re-entrench*. Meanwhile, since A also "shrinks" towards the unstable manifold by the action of P^n, there will continue to be a part of $P^n(A)$ which remains within A. Therefore, the set $P^n(A) \cap A$ will consist of at least two strips as shown on the right in Fig. 3. While A is *not* a rectangle as in the usual horseshoe construction [Alligood *et al.*, 1996; Robinson, 1999; Bollt & Santitissadeekorn, 2013], this process generates an embedded horseshoe [Robinson, 1999; Bollt & Santitissadeekorn, 2013]. Define the map $T = P^n$, and let $\Gamma = \bigcap_{i=-\infty}^{\infty} T^i(A)$. Then $T : \Gamma \to \Gamma$ is semi-conjugate to a Bernoulli shift map on two-symbols, $s : \Sigma_2 \to \Sigma_2$, with details in standard references. We have claimed only semi-conjugacy since without showing uniform contraction, then it is possible that many points are symbolized by one symbolic sequence. ■

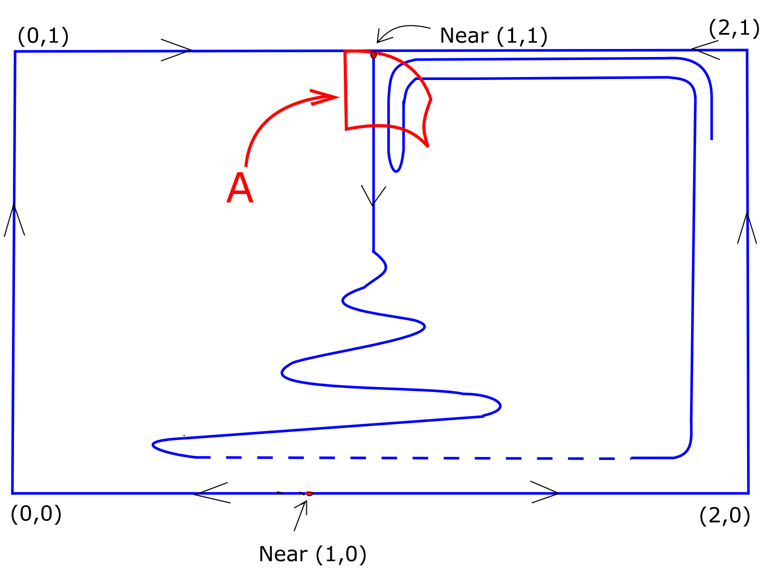

(a)

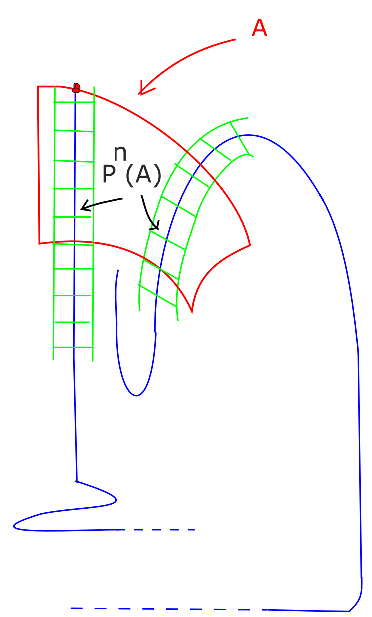

(b)

Fig. 3. A topological horseshoe embedded in the Double-Gyre. (a) As described in proof of Theorem 5, a topological rectangle set labeled A and shown in red, can be defined transversally to the re-entrenchment region and (b) there is a time $n > 0$ such that $P^n(A) \cap A$ has stretched into two branches.

Notice that this presentation of an embedded horseshoe is by direct construction, rather than the usual Smale–Birkhoff theorem that follows showing a transverse intersection of stable and unstable manifolds, which fails for reasons already described. Instead we have relied largely on the re-entrenchment theorem.

3. Folding Defined by Curvature in the Double-Gyre Flow

We have established the existence of chaos in the Double-Gyre system for small enough ε. The crux of this argument comes from the lobes re-entrenching. Now, these lobes are specifically formed through the *folding of the manifolds*. The relevance of folding is less studied than stretching (for which, for example, finite-time Lyapunov exponents [Shadden *et al.*, 2005; Allshouse & Peacock, 2015; Brunton & Rowley, 2010; Lipinski & Mohseni, 2010; Garaboa-Paz & Perez-Munuzuri, 2015; Balasuriya *et al.*, 2016] are a valuable tool), though both contribute toward chaotic transport. In this section, we follow a recently emerging idea [Ma *et al.*, 2016; Gajamannage & Bollt, 2016] of examining the folding process in terms of curvature of the manifolds. Specifically, we follow the points of high curvature in determining where the "folding is generated," and the "stretching" of the regions in-between. Thus, we highlight how stretching and folding interplay in generating the horseshoe-driven chaotic motion in the Double-Gyre. We use both analytical and numerical methods in this analysis, and obtain similar results.

The analytical expressions in (3) and (5) allow for a $\mathcal{O}(\varepsilon)$ parametric representation of the primary segments of the stable and unstable manifolds, in terms of the parameter p, at each fixed time t. These expressions enable the determination of the location of fold points, distance between points on each manifold, and also the curvature at each point on the manifold, as shown in Appendix D. Since $x_2^s(p)$ is monotonic in p, fold points can simply be obtained by examining turning points of $x_1^s(p)$ with respect to p; these also represent turning points with respect to the variable x_2^s. We show in Fig. 4 the first four fold points of the stable manifold,[1] as shown by the dots in (a). The locations of these in (x_1, x_2)-space are shown in Fig. 5, where (b) presents a close-up view of (a). The same color-coding is used for the four points in both Figs. 4 and 5. We note that, because the stable manifold curve must intersect the unstable manifold curve (not shown in Fig. 5, but this emanates downwards from near $(1, 1)$) infinitely many times, there must be infinitely many fold points. We only show the first four, since by Theorem 2 the approximation (4) breaks down in the limit $p \to -\infty$. This is because the stable manifold

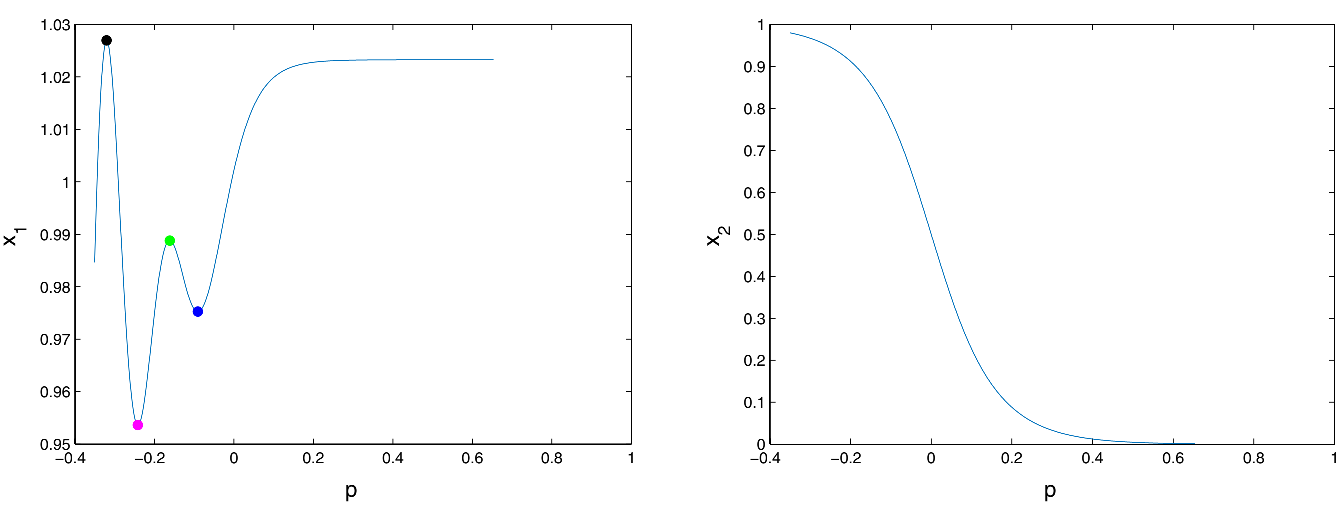

(a) $x_1^s(p)$

(b) $x_2^s(p)$

Fig. 4. Identification of the first four fold points in the stable manifold, with parameters $A = 1$, $\omega = 40$, $\varepsilon = 0.1$ and $t = 0$.

[1]Bearing in mind that $p \to \infty$ approaches the hyperbolic trajectory $\mathbf{x}_h^s(t)$, these correspond to the largest p values for which dx_1^s/dp is zero.

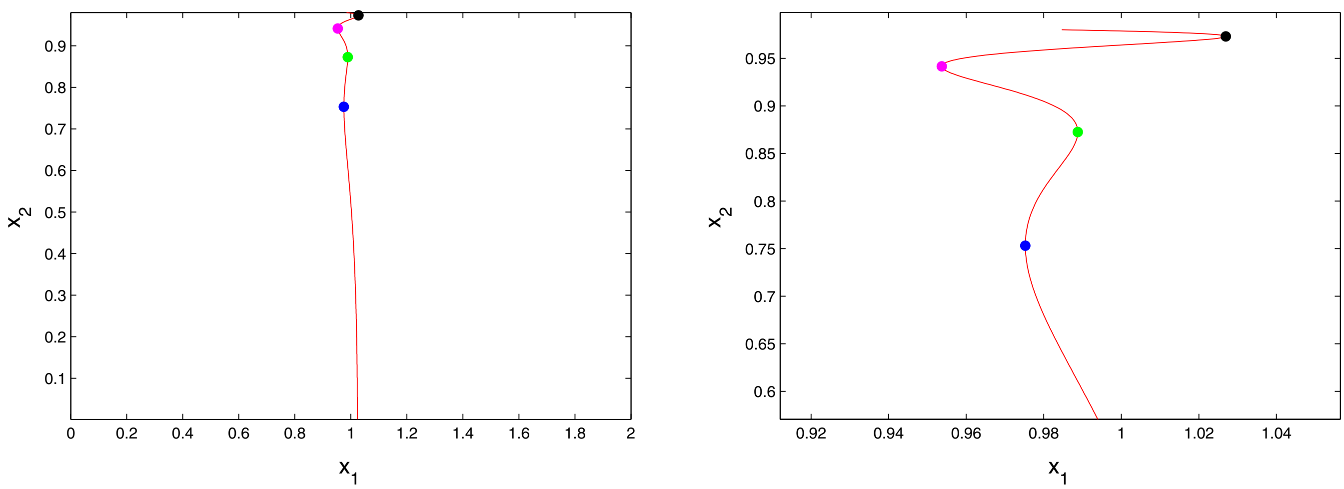

(a) Full space (b) Close-up

Fig. 5. The four fold points determined in Fig. 4, illustrated in (x_1, x_2)-space.

extends outwards and is impacted by swirling around the boundaries of the Double-Gyre, whereas the expression (4) is only locally valid near $x_1 = 1$.

In this case we have worked with analytical expressions, and have the advantage of knowing that the turning points of x_1^s with respect to p are equivalent to the turning points with respect to x_2^s. General stable manifold curves will not display such behavior (and indeed, neither does this, if taking more negative p values or increasing ε further). We propose as a more general way of determining the folding points the *points at which the curvature exhibits a marked maximum*. We illustrate the usage of this criterion in Fig. 6, computed at the same parameter values as Fig. 4, in which we show the logarithm of the curvature in terms of p [using (D.5)] and also arclength [using also (D.4)]. The same four points identified in Figs. 4 and 5 are shown in this figure. When proceeding from right to left, i.e. from the hyperbolic trajectory near $(1, 0)$ in Fig. 5, we can see that the curvature is initially close to zero, corresponding to the almost straight line emanating from the hyperbolic trajectory. Then, the first [blue] foldpoint emerges as a local maximum point in curvature. The next high-curvature points have increasingly larger values, and also increasingly sharper peaks, in the curvature plot of Fig. 6.

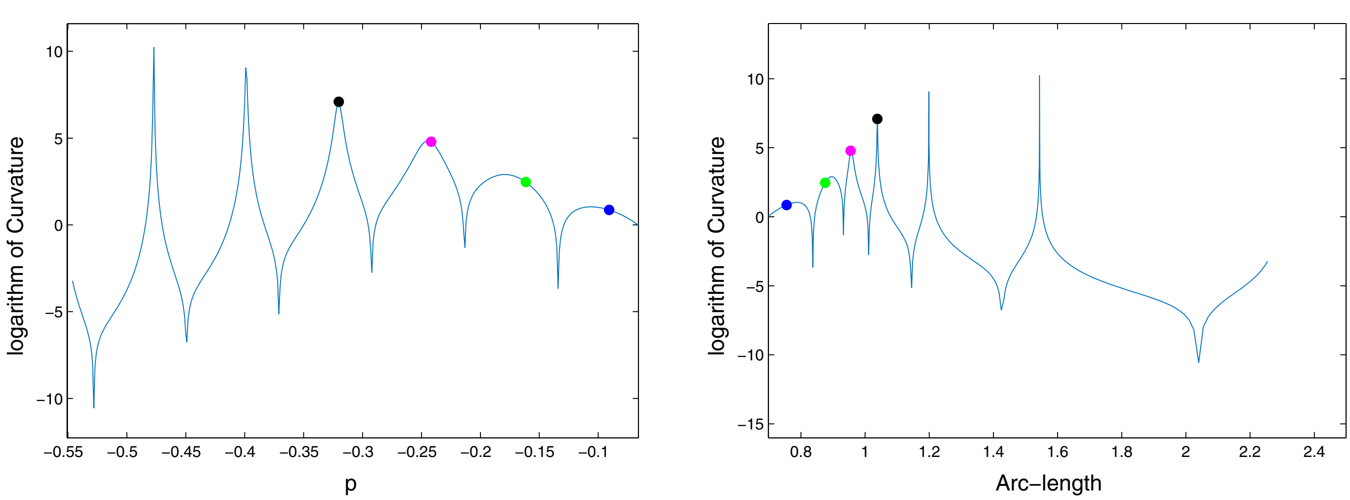

(a) (b)

Fig. 6. The logarithm of the curvature along the stable manifold plotted against (a) p and (b) arclength, at the same parameter values as in Figs. 4 and 5.

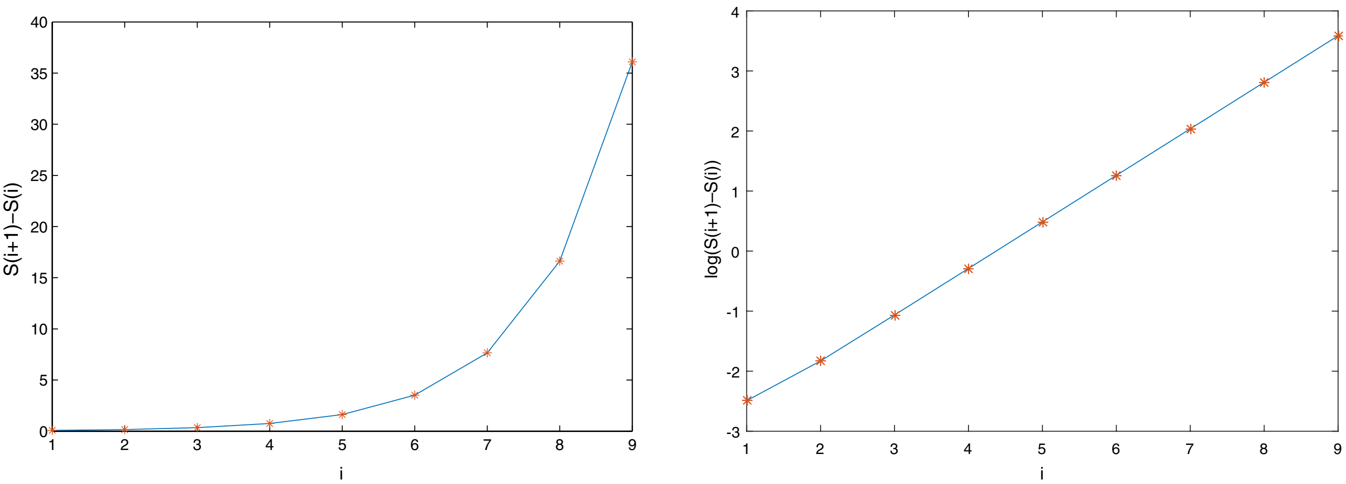

(a) (b)

Fig. 7. (a) The difference of arclength at two consecutive folding points plotted against the ith folding point and (b) the logarithm of the difference of arclength at two consecutive folding points plotted against the ith folding point, at the same parameter values as in Figs. 4–6.

Note that in Fig. 6, we used different p range than in Figs. 4 and 5 to capture more peak points of curvature. We computed the arclength in Fig. 6 with respect to the point $p = 41.7151$ and the absolute value of arclength is used for the x-axis. According to Fig. 6(a), we can observe more extremes of curvature as p move towards negative infinity. From Fig. 6(b), we notice that as we proceed along the arclength, the peaks of curvature become larger and the space between two nearest peak points is increased.

We used ten consecutive folding points (the first at $p = -0.2417$, and the tenth at $p = -0.9485$) from the range $(-1, 0)$ to create Fig. 7. In Fig. 7, the arclength (S_i) at the ith folding point is computed by taking the integral from the point $p = 41.7151$ to the ith folding point, and here we used absolute value of the arclength. These figures give an idea about the arclength distance between folding points. Figure 7(b) fits a perfect line in logarithmic scale with the slope of $m = 0.7663$ by using linear regression. We can conclude from these results

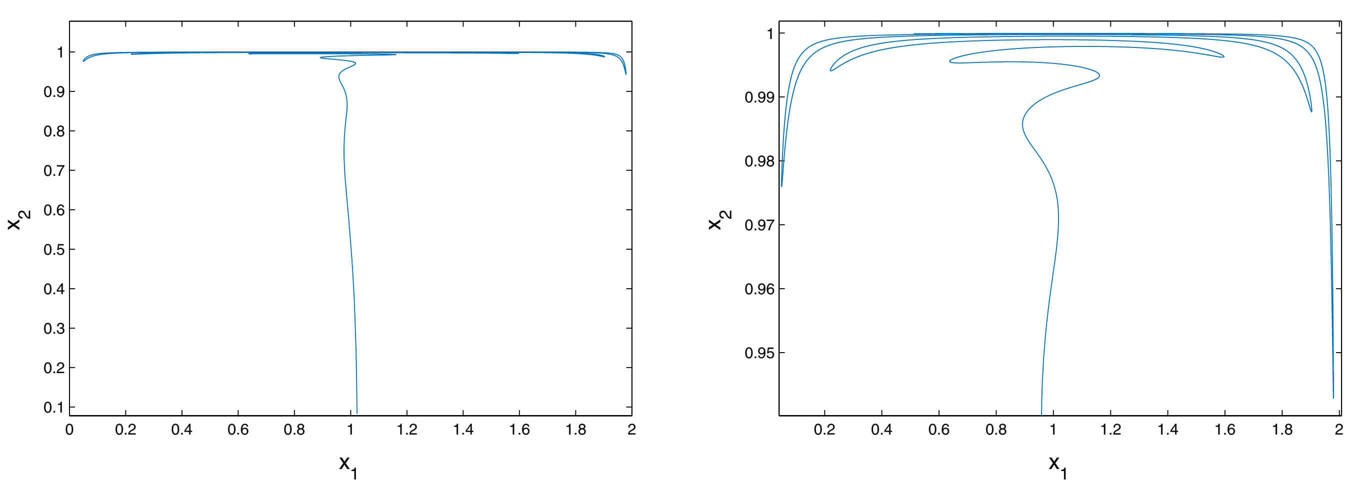

(a) (x_1, x_2) full-space (b) Close-up

Fig. 8. The stable manifold with the parameter values of the numerical method, $N = 100\,000$ and $\omega = 40$, in (a) (x_1, x_2)-phase space and (b) zoomed around $x_2 = 1$.

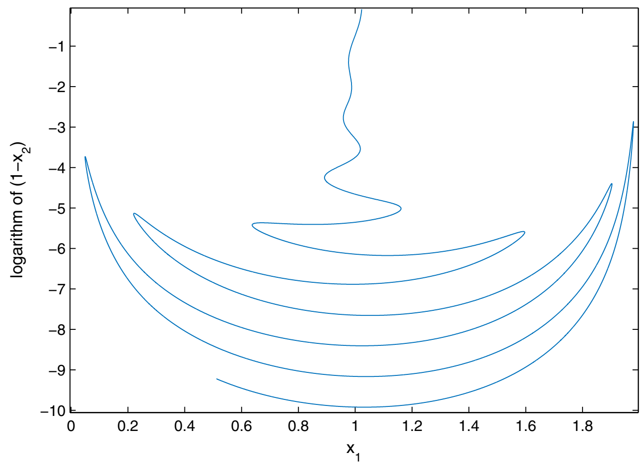

Fig. 9. The stable manifold with the parameter values of the numerical method, $N = 100\,000$ and $\omega = 40$, in $(x_1, \ln(1 - x_2))$-space (to elucidate the structure).

that the arclength between two consecutive folding points grow exponentially, when p moves toward the negative infinity.

From Fig. 10, we can notice that as we proceed along the arclength, the extremes of curvature become progressively larger due to folded lobes squeezing between lobes as seen in Fig. 8, but spaced progressively further apart, between relatively flat segments, and the near zero curvature points are inflection points.

We note that Figs. 8–10 were plotted numerically and we used same parameter values as in Figs. 4–7 with $N = 100\,000$. Here N is the number of sampling points of the function.

From this study, we can conclude that there were infinitely many folding points around $x_2 = 1$ along the stable manifold and there were infinitely many folding points around $x_2 = 0$ along the unstable manifold. We were able to see that the curvature became high at each folding point and these high-curvature values were increased when the stable manifold approached $x_2 = 1$. Also we were able to figure out that the arclength between two nearest folding points was increased, when the stable manifold approached $x_2 = 1$.

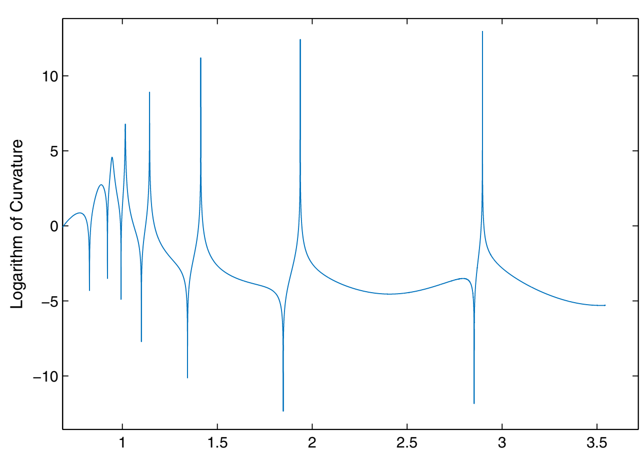

Fig. 10. The logarithm of curvature with respect to the arclength, when $N = 100\,000$, $\omega = 40$.

4. Concluding Remarks

In this paper, we have specifically addressed the concept of folding, particularly in relation to the Double-Gyre flow. The folds in the stable and unstable manifolds were used to construct a horseshoe map in this flow, and thereby prove the implicitly accepted fact that the system is chaotic. We also show how tracking the curvature is an excellent method for characterizing folding. In highlighting the role of folding, we have addressed an aspect of chaos which is seldom quantified.

Acknowledgments

S. Balasuriya acknowledges support from the Australian Research Council through grant FT130100484, and travel support from the University of Adelaide and Clarkson University during his visit to Clarkson when this work was initiated. E. Bollt is supported by, the Army Research Office, N68164-EG and W911NF-12-1-0276, and the ONR N00014-15-1-2093, and the NGA, and K. G. D. Sulalitha Priyankara is supported directly by Clarkson University.

References

Alligood, K., Sauer, T. & Yorke, J. [1996] *Chaos*: *An Introduction to Dynamical Systems* (Springer-Verlag, NY).

Allshouse, M. & Peacock, T. [2015] "Lagrangian based methods for coherent structure detection," *Chaos* **25**, 097617.

Arrowsmith, D. & Vivaldi, F. [1993] "Some p-adic representations of the Smale horseshoe," *Phys. Lett. A* **176**, 292–294.

Balasuriya, S. [2005a] "Direct chaotic flux quantification in perturbed planar flows: General time-periodicity," *SIAM J. Appl. Dyn. Syst.* **4**, 282–311.

Balasuriya, S. [2005b] "Optimal perturbation for enhanced chaotic transport," *Physica D* **202**, 155–176.

Balasuriya, S. [2006] "Cross-separatrix flux in time-aperiodic and time-impulsive flows," *Nonlinearity* **19**, 2775–2795.

Balasuriya, S. [2011] "A tangential displacement theory for locating perturbed saddles and their manifolds," *SIAM J. Appl. Dyn. Syst.* **10**, 1100–1126.

Balasuriya, S. [2014] "Nonautonomous flows as open dynamical systems: Characterising escape rates and time-varying boundaries," *Ergodic Theory, Open Dynamics, and Coherent Structures*, Springer Proc. Mathematics and Statistics, Vol. 70 (Springer), pp. 1–30.

Balasuriya, S. [2016a] *Barriers and Transport in Unsteady Flows: A Melnikov Approach*, Mathematical Modeling and Computation (SIAM Press, Philadelphia).

Balasuriya, S. [2016b] "Local stable and unstable manifolds and their control in nonautonomous finite-time flows," *J. Nonlin. Sci.* **26**, 895–927.

Balasuriya, S. & Ouellette, N. [2016] "Hyperbolic neighborhoods as organizers of finite-time exponential stretching," *APS Division of Fluid Dynamics Meeting Abstracts*.

Balasuriya, S., Kalampattel, R. & Ouellette, N. [2016] "Hyperbolic neighbourhoods as organizers of finite-time exponential stretching," *J. Fluid Mech.* **807**, 509–545.

Balibrea, F. & Snoha, L. [2003] "Topological entropy of Devaney chaotic maps," *Topol. Appl.* **133**, 225–239.

Battelli, F. & Lazzari, C. [1986] "Exponential dichotomies, heteroclinic orbits and Melnikov functions," *J. Diff. Eqs.* **86**, 342–366.

Bertozzi, A. [1988] "Heteroclinic orbits and chaotic dynamics in planar fluid flows," *SIAM J. Math. Anal.* **19**, 1271–1294.

Blazevski, D. & Haller, G. [2014] "Hyperbolic and elliptic transport barriers in three-dimensional unsteady flows," *Physica D* **273**, 46–62.

Bollt, E. [2000] "Controlling chaos and the inverse Frobenius–Perron problem: Global stabilization of arbitrary invariant measures," *Int. J. Bifurcation and Chaos* **10**, 1033–1050.

Bollt, E., Billings, L. & Schwartz, I. [2002] "A manifold independent approach to understanding transport in stochastic dynamical systems," *Physica D* **173**, 153–177.

Bollt, E., Luttman, A., Kramer, S. & Basnayake, R. [2012] "Measurable dynamics analysis of transport in the Gulf of Mexico during the oil spill," *Int. J. Bifurcation and Chaos* **22**, 1230012-1–12.

Bollt, E. & Santitissadeekorn, N. [2013] *Applied and Computational Measurable Dynamics*, Mathematical Modeling and Computation (SIAM Press, Philadelphia).

BozorgMagham, A. & Ross, S. [2015] "Atmospheric Lagrangian coherent structures considering unresolved turbulence and forecast uncertainty," *Commun. Nonlin. Sci. Numer. Simul.* **22**, 964–979.

Branicki, M. & Wiggins, S. [2010] "Finite-time Lagrangian transport analysis: Stable and unstable manifolds of hyperbolic trajectories and finite-time Lyapunov exponents," *Nonlin. Proc. Geophys.* **17**, 1–36.

Brunton, S. & Rowley, C. [2010] "Fast computation of finite-time Lyapunov exponent fields for unsteady flows," *Chaos* **20**, 017503.

Budisic, M. & Mezic, I. [2012] "Geometry of the ergodic quotient reveals coherent structures in flows," *Physica D* **241**, 1255–1269.

Chen, Y. [2006] "Smale horseshoe via the anti-integrability," *Chaos Solit. Fract.* **28**, 377–385.

Coppel, W. [1978] *Dichotomies in Stability Theory*, Lecture Notes in Mathematics (Springer-Verlag, Berlin).

Dellnitz, M. & Junge, O. [2002] "Set oriented numerical methods for dynamical systems," *Handbook of Dynamical Systems*, Vol. 2 (North-Holland, Amsterdam), pp. 221–264.

Duc, L. & Siegmund, S. [2008] "Hyperbolicity and invariant manifolds for planar nonautonomous systems on finite time intervals," *Int. J. Bifurcation and Chaos* **18**, 641–674.

Farazmand, M. & Haller, G. [2013] "Attracting and repelling Lagrangian coherent structures from a single computation," *Chaos* **23**, 023101.

Froyland, G., Padberg-Gehle, K., England, M. & Treguier, A. [2007] "Detection of coherent oceanic structures via transfer operators," *Phys. Rev. Lett.* **98**, 224503.

Froyland, G. & Padberg-Gehle, K. [2009] "Almost-invariant sets and invariant manifolds connecting probabilistic and geometric descriptions of coherent structures in flows," *Physica D* **238**, 1507–1523.

Froyland, G., Santitissadeekorn, N. & Monahan, A. [2010] "Transport in time-dependent dynamical systems: Finite-time coherent sets," *Chaos* **20**, 043116.

Froyland, G. & Padberg-Gehle, K. [2012] "Finite-time entropy: A probabilistic approach for measuring nonlinear stretching," *Physica D* **241**, 1612–1628.

Froyland, G. [2013] "An analytic framework for identifying finite-time coherent sets in time-dependent dynamical systems," *Physica D* **250**, 1–19.

Froyland, G. & Padberg-Gehle, K. [2015] "A rough-and-ready cluster-based approach for extracting finite-time coherent sets from sparse and incomplete trajectory data," *Chaos* **25**, 087406.

Gajamannage, K. & Bollt, E. [2016] "Detecting phase transitions in collective motion using manifold's curvature," *Math. Biosci. Engin.* **14**, 437–453.

Garaboa-Paz, D. & Perez-Munuzuri, V. [2015] "A method to calculate finite-time Lyapunov exponents for intertial particles in incompressible flows," *Nonlin. Proc. Geophys.* **22**, 571–577.

Guckenheimer, J. & Holmes, P. [1983] *Nonlinear Oscillations, Dynamical Systems and Bifurcations of Vector Fields* (Springer, NY).

Hadjighasem, A., Karrasch, D., Teramoto, H. & Haller, G. [2016] "Spectral-clustering approach to Lagrangian vortex detection," *Phys. Rev. E* **93**, 063107.

Haller, G. & Yuan, G. [2000] "Lagrangian coherent structures and mixing in two-dimensional turbulence," *Physica D* **147**, 352–370.

Haller, G. [2015] "Lagrangian coherent structures," *Ann. Rev. Fluid Mech.* **47**, 137–162.

He, G., Pan, C., Feng, L., Gao, Q. & Wang, J. [2016] "Evolution of Lagrangian coherent structures in a cylinder-wake disturbed flat plate boundary layer," *J. Fluid Mech.* **792**, 274–306.

Holmes, P. [1986] "Knotted periodic orbits in suspensions of Smale's horseshoe: Period multiplying and cabled knots," *Physica D* **21**, 7–41.

Holmes, P. [1990] "Poincaré, celestial mechanics, dynamical-systems theory and chaos," *Phys. Rep.* **193**, 137–163.

Huntley, H., Lipphardt, B., Jacobs, G. & Kirwan, A. [2015] "Clusters, deformation, and dilation: Diagnostics for material accumulation regions," *J. Geophys. Res.: Oceans* **120**, 6622–6636.

Johnson, P. & Meneveau, C. [2015] "Large-deviation joint statistics of the finite-time Lyapunov spectrum in isotropic turbulence," *Phys. Fluids* **27**, 085110.

Ju, N., Small, D. & Wiggins, S. [2003] "Existence and computation of hyperbolic trajectories of aperiodically time dependent vector fields and their approximations," *Int. J. Bifurcation and Chaos* **13**, 1449–1457.

Karrasch, D., Farazmand, M. & Haller, G. [2015] "Attraction-based computation of hyperbolic Lagrangian coherent structures," *J. Comput. Dyn.* **2**, 83–93.

Kelley, D., Allshouse, M. & Ouellette, N. [2013] "Lagrangian coherent structures separate dynamically distinct regions in fluid flows," *Phys. Rev. E* **88**, 013017.

Lipinski, D. & Mohseni, K. [2010] "A ridge tracking algorithm and error estimate for efficient computation of Lagrangian coherent structures," *Chaos* **20**, 017504.

Ma, T. & Bollt, E. [2013] "Relatively coherent sets as a hierarchical partition method," *Int. J. Bifurcation and Chaos* **23**, 1330026-1–17.

Ma, T. & Bollt, E. [2014] "Differential geometry perspective of shape coherence and curvature evolution by finite-time nonhyperbolic splitting," *SIAM J. Appl. Dyn. Syst.* **13**, 1106–1136.

Ma, T. & Bollt, E. [2015] "Shape coherence and finite-time curvature evolution," *Int. J. Bifurcation and Chaos* **25**, 1550076-1–10.

Ma, T., Ouellette, N. & Bollt, E. [2016] "Stretching and folding in finite time," *Chaos* **26**, 023112.

Mancho, M., Small, D., Wiggins, S. & Ide, K. [2003] "Computation of stable and unstable manifolds of hyperbolic trajectories in two-dimensional, aperiodically time-dependent vector fields," *Physica D* **182**, 188–222.

Mancho, A., Wiggins, S., Curbelo, J. & Mendoza, C. [2013] "Lagrangian descriptors: A method for revealing phase space structures of general time dependent dynamical systems," *Commun. Nonlin. Sci. Numer. Simul.* **18**, 3530–3557.

McIlhany, K. & Wiggins, S. [2012] "Eulerian indicators under continuously varying conditions," *Phys. Fluids* **24**, 073601.

Melnikov, V. [1963] "On the stability of the centre for time-periodic perturbations," *Trans. Moscow Math. Soc.* **12**, 1–56.

Mezic, I., Loire, S., Fonoberov, V. & Hogan, P. [2010] "A new mixing diagnostic and Gulf oil spill movement," *Science* **330**, 486–489.

Mosovsky, B. & Meiss, J. [2011] "Transport in transitory dynamical systems," *SIAM J. Appl. Dyn. Syst.* **10**, 35–65.

Muller-Karger, C., Mirena, A. & Lopez, J. [2000] "Hyperbolic trajectories for pick-and-place operations to elude obstacles," *IEEE Trans. Robot. Automat.* **16**, 294–300.

Namikawa, J. & Hashimoto, T. [2004] "Dynamics and computation in functional shifts," *Nonlinearity* **17**, 1317.

Nelson, D. & Jacobs, G. [2015] "DG-FTLE: Lagrangian coherent structures with high-order discontinuous-Galerkin methods," *J. Comput. Phys.* **295**, 65–86.

Nevins, T. & Kelley, D. [2016] "Optimal stretching in advection–reaction–diffusion systems," *Phys. Rev. Lett.* **117**, 164502.

Onu, K., Huhn, F. & Haller, G. [2015] "{LCS} Tool: A computational platform for Lagrangian coherent structures," *J. Comput. Sci.* **7**, 26–36.

Palmer, K. [1984] "Exponential dichotomies and transversal homoclinic points," *J. Diff. Eqs.* **55**, 225–256.

Poje, A., Haller, G. & Mezic, I. [1999] "The geometry and statistics of mixing in aperiodic flows," *Phys. Fluids* **11**, 2963–2968.

Pratt, K., Meiss, J. & Crimaldi, J. [2015] "Reaction enhancement of initially distant scalars by Lagrangian coherent structures," *Phys. Fluids* **27**, 035106.

Robinson, C. [1999] *Dynamical Systems: Stabiliy, Symbolic Dynamics and Chaos*, Studies in Advanced Mathematics (CRC Press).

Rom-Kedar, V., Leonard, A. & Wiggins, S. [1990] "An analytical study of transport, mixing and chaos in an unsteady vortical flow," *J. Fluid Mech.* **214**, 347–394.

Rom-Kedar, V. & Poje, A. [1999] "Universal properties of chaotic transport in the presence of diffusion," *Phys. Fluids* **11**, 2044–2057.
Rosi, G., Walker, A. & Rival, D. [2015] "Lagrangian coherent structure identification using a Voronoi tessellation-based networking algorithm," *Exp. Fluids* **56**, 189.
Rössler, O. [1977] "Horseshoe-map chaos in the Lorenz equation," *Phys. Lett. A* **60**, 392–394.
Sattari, S., Chen, Q. & Mitchell, K. [2016] "Using heteroclinic orbits to quantify topological entropy in fluid flows," *Chaos* **26**, 033112.
Shadden, S., Lekien, F. & Marsden, J. [2005] "Definition and properties of Lagrangian coherent structures from finite-time Lyapunov exponents in two-dimensional aperiodic flows," *Physica D* **212**, 271–304.
Sudharsan, M., Brunton, S. & Riley, J. [2016] "Lagrangian coherent structures and inertial particle dynamics," *Phys. Rev. E* **93**, 033108.
Tallapragada, P. & Ross, S. [2013] "A set-oriented defintion of finite-time Lyapunov exponents and coherent sets," *Commun. Nonlin. Sci. Numer. Simul.* **18**, 1106–1126.
Teramoto, H., Haller, G. & Komatsuzaki, T. [2013] "Detecting invariant manifolds as stationary LCSs in autonomous dynamical systems," *Chaos* **23**, 043107.
Tumasz, S. & Thiffeault, J. [2013] "Estimating topological entropy from the motion of stirring rods," *Procedia IUTAM* **7**, 117–126.
Vleck, E. V. [1994] "Numerical shadowing near hyperbolic trajectories," *SIAM J. Sci. Comput.* **16**, 1177–1189.
Wiggins, S. [1992] *Chaotic Transport in Dynamical Systems* (Springer-Verlag, NY).
Wiggins, S. & Mancho, A. M. [2014] "Barriers to transport in aperiodically time-dependent two-dimensional velocity fields: Nekhoroshev's theorem and "Nearly Invariant" tori," *Nonlin. Proc. Geophys.* **21**, 165–185.
Williams, M., Rypina, I. & Rowley, C. [2015] "Identifying finite-time coherent sets from limited quantities of Lagrangian data," *Chaos* **25**, 087408.

Appendix A

Proof of Theorem 1 (Heteroclinic Intersections)

The standard method in these situations is to use the Melnikov technique [Melnikov, 1963; Guckenheimer & Holmes, 1983; Balasuriya, 2014], which is a perturbative technique with respect to ε. We will work with the nonautonomous approach as detailed in [Balasuriya, 2016a] in particular, whose approach is to imagine the manifolds as being parametrized by time t continuously. This requires writing (1) in the perturbed form

$$\dot{\mathbf{x}} = \mathbf{f}(\mathbf{x}) + \varepsilon\mathbf{g}(\mathbf{x}, t) + \mathcal{O}(\varepsilon^2)$$

in which $\mathbf{x} = (x, y)$, and the $\mathcal{O}(\varepsilon^2)$ term is uniformly bounded on $\Omega \times \mathbb{R}$. Taylor expansions of (1) enable the identifications

$$\mathbf{f}(x, y) = \begin{pmatrix} -\pi A \sin(\pi x)\cos(\pi y) \\ \pi A \cos(\pi x)\sin(\pi y) \end{pmatrix}$$

and

$$\mathbf{g}(x, y, t) = \begin{pmatrix} -\pi^2 A(x^2 - 2x)\cos(\pi y)\cos(\pi x) \\ \pi A \sin(\pi y)[2\cos(\pi x)(x-1) - \pi(x^2 - 2x)\sin(\pi x)] \end{pmatrix} \sin(\omega t).$$

Here, we follow the methodology of quantifying the signed distance between the perturbed manifolds at a location $\bar{\mathbf{x}}(p) = (1, \bar{x}_2(p))$ on the unperturbed heteroclinic. At a general time t, the vector from the stable to the unstable manifold, going through this point and pointing in the x_1-direction, can be expressed by

$$d(p, t) = \varepsilon \frac{M(p, t)}{|\mathbf{f}(\bar{\mathbf{x}}(p))|} + \mathcal{O}(\varepsilon^2), \tag{A.1}$$

valid for $p \in [-P, P]$ and $t \in [-T, T]$, for P, T finite. This is a signed distance, which is positive if the vector points in the $+x_1$-direction, and the Melnikov function in this interpretation is given by [Balasuriya, 2016a, 2014, 2006]

$$M(p, t) = \int_{-\infty}^{\infty} \mathbf{f}(\bar{\mathbf{x}}(\tau)) \wedge \mathbf{g}(\bar{\mathbf{x}}(\tau), \tau + t - p)\mathrm{d}\tau$$

with the wedge product defined by $\mathbf{f} \wedge \mathbf{g} := f_1 g_2 - f_2 g_1$ in component form. Now, substituting the relevant $\mathbf{f}$ and $\mathbf{g}$, inserting $\bar{\mathbf{x}}(\tau) = (1, \bar{x}_2(\tau))$, and simplifying leads to

$$\begin{aligned} M(p, t) &= \pi^3 A^2 \int_{-\infty}^{\infty} \tanh(\pi^2 A\tau)\,\mathrm{sech}\,(\pi^2 A\tau) \\ &\quad \times \sin[\omega(\tau + t - p)]\mathrm{d}\tau \\ &= \omega\,\mathrm{sech}\,\frac{\omega}{2\pi A}\sin[\omega(t - p)] \\ &=: R(\omega)\sin[\omega(t - p)], \end{aligned} \tag{A.2}$$

where the final simplification (A.2) is obtainable by writing $\sin[\omega(\tau+t-p)] = \sin[\omega(t-p)]\cos(\omega\tau) + \cos[\omega(t-p)]\sin(\omega\tau)$ and splitting the integrals [Balasuriya, 2014, 2005a, 2005b, etc.], and performing the one nonzero integral that results. At each fixed t, $M(p,t)$ clearly has nonsimple zeros when $p = t - m\pi/\omega$, $m \in \mathbb{Z}$. From (A.1), this indicates that $d(p,t)$ has nearby zeros for small enough $|\varepsilon|$. Thus, the stable and unstable manifolds intersect — infinitely many times, in fact — in each time slice. This leads to a heteroclinic tangle near $x_1 = 1$, resulting in complicated transport between the gyres. This transport can be quantified to leading-order in ε as an *instantaneous flux* [Balasuriya, 2016a, 2014, 2006] from the left to the right gyre by

$$\varepsilon M(p,t) = \varepsilon R(\omega)\sin[\omega(t-p)], \tag{A.3}$$

as an *average flux* [Rom-Kedar & Poje, 1999] by $\varepsilon R(\omega)$, or (in terms of lobes created through the intersections) as a *lobe area* [Rom-Kedar *et al.*, 1990; Wiggins, 1992] of $\varepsilon R(\omega)2\pi/\omega$. ■

Appendix B
Proof of Theorem 2 (Stable Manifold)

This proof relies on the expressions for the perturbed stable manifold obtained in Theorem 2.7 in [Balasuriya, 2011] and Theorem 2 in [Balasuriya, 2014]. While those results are derived for the more general situation of *compressible* flows which are not necessarily time-periodic, these relaxations are not necessary in the present context. Using the notation already introduced in the proof of Theorem 1, the stable manifold at a time t can be represented parametrically by

$$\mathbf{x}^s(p,t) = \overline{\mathbf{x}}(p) + \varepsilon\left[\frac{M^s(p,t)}{|\mathbf{f}(\overline{\mathbf{x}}(p))|^2}\mathbf{f}^\perp(\overline{\mathbf{x}}) + \frac{B^s(p,t)}{|\mathbf{f}(\overline{\mathbf{x}}(p))|^2}\mathbf{f}(\overline{\mathbf{x}})\right] + \mathcal{O}(\varepsilon^2)$$

for $p \in [P,\infty)$ (any P which is finite), in which the $\perp$ notation indicates the rotation of a vector by $+\pi/2$, and expressions for M^s and B^s will be given shortly. In this case, since $\overline{\mathbf{x}}(p)$, the unperturbed stable manifold, simply lies along the line $x_1 = 1$, the velocity $\mathbf{f}$ along it is directly in the negative y-direction. Thus, $\mathbf{f}^\perp$ is simply the component of $\mathbf{f}$ in the $+x_1$-direction. Now, the Melnikov function M^s is given by

$$M^s(p,t) = \int_p^\infty \mathbf{f}(\overline{\mathbf{x}}(\tau)) \wedge \mathbf{g}(\overline{\mathbf{x}}(\tau), \tau+t-p)\mathrm{d}\tau,$$

this therefore represents the perturbation of the stable manifold in the *normal* direction to the original manifold. The tangential perturbation is given by the function

$$B^s(p,t) := |\mathbf{f}(\overline{\mathbf{x}}(p))|^2 \int_0^p \frac{R^s(\tau)M^s(p,\tau+t-p) + \mathbf{f}(\overline{\mathbf{x}}(\tau))\cdot\mathbf{g}(\overline{\mathbf{x}}(\tau),\tau+t-p)}{|\mathbf{f}(\overline{\mathbf{x}}(\tau))|^2}\mathrm{d}\tau,$$

where

$$R^s(\xi) := \frac{(\mathbf{f}^\perp)^\top(\overline{\mathbf{x}}(\xi))[(D\mathbf{f})^\top(\overline{\mathbf{x}}(\xi)) + (D\mathbf{f})(\overline{\mathbf{x}}(\xi))]\mathbf{f}(\overline{\mathbf{x}}(\xi))}{|\mathbf{f}(\overline{\mathbf{x}}(\xi))|^2}.$$

We immediately dispense with the more complicated tangential displacement since it is easy to verify that for the Double-Gyre, $R^s \equiv 0$ and $\mathbf{f}\cdot\mathbf{g} \equiv 0$. Therefore, there is no change to the x_2-coordinate, and we can write using (2) that $x_2^s(p,t) = \overline{x}_2(p) = \frac{2}{\pi}\cot^{-1} e^{\pi^2 Ap}$. Using the results derived in the proof of Theorem 1, we can write the Melnikov function as

$$M^s(p,t) = \pi^3 A^2 \int_p^\infty \tanh(\pi^2 A\tau)\,\mathrm{sech}\,(\pi^2 A\tau) \times \sin[\omega(\tau+t-p)]\mathrm{d}\tau$$

which cannot be evaluated in terms of simple functions,[2] unlike in (A.2). Next, using $\overline{\mathbf{x}}(p)$ as given in (2), we have

$$\mathbf{f}(\overline{\mathbf{x}}(p)) = \begin{pmatrix} 0 \\ \pi A\sin(\pi\overline{x}_2(p)) \end{pmatrix} = \begin{pmatrix} 0 \\ \pi A\,\mathrm{sech}\,(\pi^2 Ap) \end{pmatrix}$$

and the stable manifold expression (4) results. The location of the hyperbolic trajectory can be obtained by appealing directly to Theorem 2.10 in [Balasuriya, 2011], but here we adopt a more

[2] It can be represented in a complicated way in terms of hypergeometric functions, but this is not particularly illuminating and hence will be avoided.

intuitive, formal, approach. We now have the x_1-coordinate of the perturbed stable manifold given by (4), which upon changing the variable of integration (and with the higher-order term neglected for convenience) can be written as

$$x_1^s(p,t) = 1 + \varepsilon\pi^2 A \int_t^\infty \frac{\tanh(\pi^2 A(\tau - t + p))\,\mathrm{sech}\,(\pi^2 A(\tau - t + p))}{\mathrm{sech}\,(\pi^2 Ap)} \sin\omega\tau \mathrm{d}\tau.$$

Since the hyperbolic trajectory is approached in the limit $p \to \infty$, applying this limit inside the integral gives

$$x_1^s(\infty,t) = 1 + \varepsilon\pi^2 A e^{\pi^2 At} \int_t^\infty e^{-\pi^2 A\tau} \sin\omega\tau \mathrm{d}\tau$$

which can be integrated and reorganized to give (3). The x_2-coordinate of the hyperbolic trajectory remains fixed at $x_2 = 0$ since it is easy to see that this line is invariant for the full flow (1). Next, the reciprocal slope of the manifold at the hyperbolic trajectory is needed. This is zero when $\varepsilon = 0$, and Theorem 2.2 can be used to prove that the $\mathcal{O}(\varepsilon)$-correction to this is zero. More intuitively, this occurs because

$$\begin{aligned}
\left.\frac{dx_1^s}{dx_2^s}\right|_{\mathbf{x}_h^s(t)} &= \lim_{p\to\infty} \frac{\dfrac{\partial x_1^s}{\partial p}}{\dfrac{\partial x_2^s}{\partial p}} = \lim_{p\to\infty} \frac{\varepsilon\pi^2 A \displaystyle\int_t^\infty \frac{d}{dp}\left[\frac{\tanh(\pi^2 A(\tau - t + p))\,\mathrm{sech}\,(\pi^2 A(\tau - t + p))}{\mathrm{sech}\,(\pi^2 Ap)}\right] \sin\omega\tau \mathrm{d}\tau}{\pi A \dfrac{d}{dp}\,\mathrm{sech}\,(\pi^2 Ap)} \\
&= \varepsilon\pi \int_t^\infty \lim_{p\to\infty} \frac{\dfrac{d}{dp}\left[\dfrac{\tanh(\pi^2 A(\tau - t + p))\,\mathrm{sech}\,(\pi^2 A(\tau - t + p))}{\mathrm{sech}\,(\pi^2 Ap)} - 1\right]}{\dfrac{d}{dp}\,\mathrm{sech}\,(\pi^2 Ap)} \sin\omega\tau \mathrm{d}\tau \\
&= \varepsilon\pi \int_t^\infty \lim_{p\to\infty} \frac{\left[\dfrac{\tanh(\pi^2 A(\tau - t + p))\,\mathrm{sech}\,(\pi^2 A(\tau - t + p))}{\mathrm{sech}\,(\pi^2 Ap)} - 1\right]}{\mathrm{sech}\,(\pi^2 Ap)} \sin\omega\tau \mathrm{d}\tau \\
&= \varepsilon\pi \int_t^\infty \lim_{p\to\infty} \frac{\tanh(\pi^2 A(\tau - t + p)) - 1}{\mathrm{sech}\,(\pi^2 Ap)} \sin\omega\tau \mathrm{d}\tau \\
&= \varepsilon\pi \int_t^\infty \lim_{p\to\infty} \frac{\mathrm{sech}^2(\pi^2 A(\tau - t + p))}{-\mathrm{sech}\,(\pi^2 Ap)\tanh(\pi^2 Ap)} \sin\omega\tau \mathrm{d}\tau = 0,
\end{aligned}$$

where we have utilized the fact that $\mathrm{sech}\,[\pi^2 A(\tau - t + p)]/\,\mathrm{sech}\,[\pi^2 Ap] \to 1$ as $p \to \infty$, and L'Hôpital's rule has been used several times. Thus, the $\mathcal{O}(\varepsilon)$ correction to the slope is zero. Given that the functions here are all uniformly bounded in suitably high norms, uniformly for $t \in \mathbb{R}$, it is clear that the $\mathcal{O}(\varepsilon^2)$ correction is bounded. ■

Appendix C

Proof of Theorem 4 (Fold Re-Entrenchment)

The outer boundaries of Ω can be easily seen to be invariant for any ε. For convenience, we only address the wrapping around ensuing from the right gyre; the left gyre also causes the identical behavior. Consider the line $x_2 = 0$, along the interface of the right gyre, that is, for $x_h^s(t) < x_1 < 2$. The flow on this satisfies

$$\dot{x}_1 = -\pi A \sin(\pi\phi(x_1,t)).$$

Now, when $\varepsilon = 0$, we have $x_h^s(t) = 1$, and ϕ goes from 1 at this value to 2 at 2. Since $\sin\pi\phi$ is negative in this range, $\dot{x}_1$ is positive in this interval. If $0 < |\varepsilon| < 1/2$, $\phi(x_1,t) = 1$ when

$$x_1 = \tilde{x} := \frac{2\varepsilon\sin\omega t - 1 + \sqrt{1 + 4\varepsilon^2\sin^2\omega t}}{2\varepsilon\sin\omega t}$$

as long as $\sin\omega t \neq 0$. (If $\sin\omega t = 0$, then $\tilde{x} = 1$.) Thus for $x_1 \in (\tilde{x}, 2)$, $\phi(x_1,t)$ lies between 1 and 2, and therefore the vector field points to the right along the lower boundary of the right gyre, in an interval near $x_1 = 2$. Using this, and a similar idea for the top of the right gyre, we can obtain the behavior as shown in Fig. 2 by the blue curves. This picture is drawn at a general time t, and the red and green represent respectively the unstable and the stable manifolds, whose behavior of this form is guaranteed by Theorems 2 and 3. Only parts of the stable manifold near $x_2 = 0$ and the unstable manifold near $x_2 = 0$ and $x_2 = 1$ are shown. While the arrows drawn on the blue bounding lines are the instantaneous directions of the velocity, those drawn on the stable/unstable manifolds are not necessarily the instantaneous velocity directions, since these manifolds, and their anchor points $\mathbf{x}_h^{s,u}(t)$, are themselves moving (mostly horizontally in the regions near $x_2 = 0$ and $x_2 = 1$). The true instantaneous velocity of particles on these manifolds is the superposition of the indicated arrows on the manifolds, and this additional motion.

Now, it must be borne in mind that the unstable manifold intersects the stable one infinitely often near $(x_h^s(t), 0)$, with the intersection points accumulating towards this instantaneous hyperbolic trajectory location. However, the lobe structures created as a result of this intersection must have equal areas, since under iteration of the Poincaré map P which samples the flow from this time t to the time $t + 2\pi/\omega$ (i.e. strobing the flow at the period of the velocity field), these lobes must get mapped to one another. The lobe with end marked by B, must get mapped to the next lobe with end marked by $P(B)$. This lobe must get thin in the x_2-direction (indeed, this width is almost not discernible in Fig. 2) because the intersection points accumulate to $(x_h^s(t), 0)$. However, the flow of (1) is incompressible, and thus area-preserving. The lobe which has $P(B)$ marked at its end must therefore have the same area as that marked with a B, and this is only achievable if it extends outwards. This extension in the x_1-direction of the unstable manifold is also implied by the formulæ for $x_1^u(p, t)$ shown in Theorem 3. One can therefore determine parts of the unstable manifold which are *arbitrarily* close to the line $x_2 = 0$, and there will be regions of this manifold which have x_1-coordinates greater than $\tilde{x}$. By continuity, the velocity at such a location can be made arbitrarily close to the velocity on $x_2 = 0$. Thus, if considering the blob marked B in Fig. 2 which is at an end of a lobe structure (where the unstable manifold folds) and assuming that this has been chosen to be within this region of influence, as time passes it will get pulled along by a velocity which is very close to that of the blue lines. Eventually, therefore, it must get pulled all the way around the right gyre, and emerge along the blue line at the top of the right gyre.

While the flow along this boundary line is to the left for x_1 near 2, we want to show something more specific: that the flow along this line approaches the hyperbolic trajectory location $x_h^u(t)$, as approximated in (5). Focus, then, on flow along this blue line, that is on the invariant line $\{x_2 = 1, 0 < x_1 < 2\}$, which obeys

$$\dot{x}_1 = \pi A \sin(\pi \phi(x_1, t)).$$

Let $z(t) = x_1(t) - x_h^u(t)$, and suppose that $x_1(0) > x_h^u(0)$. Since trajectories cannot cross on this one-dimensional phase space, it is clear that $x_1(t) > x_h^u(t)$ for $t > 0$. Now $0 < x_h(t) < x_1(t) < 2$ because the end points 0 and 2 are fixed points of the above, even if the flow is nonautonomous. Therefore $0 < z(t) < 2$, and $z(t)$ can be shown to satisfy the differential equation

$$\begin{aligned}
\dot{z} &= 2\pi A \sin\left[\frac{\pi z}{2} + \frac{\varepsilon \pi z \sin \omega t}{2}(x_1 + x_h^u - 2)\right] \\
&\quad \times \cos\left[\frac{\pi(x_1 + x_h^u)}{2} + \frac{\varepsilon\pi(x_1 + x_h^u)\sin\omega t}{2}\right. \\
&\quad \left. \times (x_1 + x_h^u - 2)\right] \\
&= -2\pi A \sin\left[\frac{\pi z}{2} + \frac{\varepsilon \pi z \sin \omega t}{2}(x_1 + x_h^u - 2)\right] \\
&\quad \times \sin\left[\frac{\pi(x_1 + x_h^u - 1)}{2} + \frac{\varepsilon\pi(x_1 + x_h^u)\sin\omega t}{2}\right. \\
&\quad \left. \times (x_1 + x_h^u - 2)\right].
\end{aligned}$$

When $\varepsilon = 0$, $x_h^u(t) = 1$, and in this situation

$$\dot{z} = -2\pi A \sin\frac{\pi z}{2} \sin\frac{\pi x_1(t)}{2} < 0,$$

whose velocity field is sign definite since both x_1 and z must lie in $(0, 2)$. Despite being nonautonomous, its solution z must decay to the fixed point $z = 0$. When $\varepsilon \neq 0$, noting also that $x_h^u = 1 + \mathcal{O}(\varepsilon)$, it is clear that one can find $|\varepsilon|$ small enough such that the sign definite nature will persist if $x_1(t)$ were chosen sufficiently close to $x_h^u(t)$. Therefore, along the blue line at the top of Fig. 2, for suitably small $|\varepsilon|$, trajectories will be attracted towards the hyperbolic trajectory $x_h^u(t)$.

Once we have this property, continuity ensures that trajectories inside Ω but near to this must also follow the behavior of proceeding towards the left. Trajectories can be made to approach $x_h^u(t)$ arbitrarily closely, by choosing trajectories which were sufficiently close to the blue line. However, the fluid blob B as shown in Fig. 2 will at some time in the future be as close as we like to the "heteroclinic network" shown in blue in Fig. 2, and thus will eventually be subject to behavior imputed for the line $x_2 = 1$. When approaching $x_h^u(t)$, this blob will therefore be subject to the unstable manifold emanating from $x_h^u(t)$, and get pulled down along it.

Consider the point u, which is at the leading-edge of the lobe marked B in Fig. 2. That is, this is a fold point. By the above argument, the flow of the Double-Gyre will ensure that its image u' will eventually be within N_δ. We want to show the existence of a fold point within N_δ. However, there is no guarantee that the point u' will also correspond to a leading-edge, i.e. a fold point. To establish the existence of a fold point, we argue that the unstable manifold must pass through u'. Now, both ends of the unstable manifold must wrap back all the way around the boundary of Ω, adjacent to the blue lines, and come back to intersect the stable manifold of $(x_h^s(t), 0)$ near to this point, since these intersection points accumulate towards $(x_h^s(t), 0)$. Hence, both ends of the unstable manifold which pass through u' must come all the way back. This ensures that there must be a fold point within N_δ; the unstable manifold must "bend back" to achieve this.

It is also instructive to think of what happens in terms of the Poincaré map and lobes. It has been argued that there are infinitely many lobes "below" the one pictured near B in Fig. 2. As one proceeds "downwards," each of these lobes is closer to the blue heteroclinic network than the previous one, and therefore subject to the motion along the network more. Thus, each successive lobe will get elongated along the network more. The end result from this process is that in N_δ, in addition to the lobe L pictured in Fig. 2, there will be an infinite number of lobes which accumulate towards the unstable manifold emanating from x_h^u. These will stretch along the unstable manifold (they cannot intersect because the lobe boundaries are themselves part of the *same* unstable manifold), and therefore will follow the undulations that the primary part of the unstable manifold has been shown to have. ■

Appendix D

Expressions from the Analytical Approximations

Here we list some expressions related to determining the curvature and fold points from the analytical approximations given by Theorems 2 and 3. At each fixed time t, the primary stable/unstable manifold curves can be thought of as being given parametrically by (4) and (6), where p is the parameter. We will only show calculations for the stable manifold, since the unstable manifold calculations are similar. By applying integration by parts and a straightforward change-of-variable to (4), the $\mathcal{O}(\varepsilon)$ expression for the x_1-coordinate of the stable manifold, given in (4), can be recast as

$$x_1^s(t) = 1 + \varepsilon \sin(\omega t) + \varepsilon\omega \cosh(\pi^2 A p) \times \int_t^\infty \operatorname{sech}[\pi^2 A(u - t + p)] \cos(\omega u) \mathrm{d}u.$$

Its derivative is therefore

$$\frac{dx_1^s}{dp} = \varepsilon\omega\pi^2 A \cosh(\pi^2 A p) \int_t^\infty \operatorname{sech}[\pi^2 A(u - t + p)] \times \{\tanh[\pi^2 A p] - \tanh[\pi^2 A(u - t + p)]\} \times \cos(\omega u) \mathrm{d}u.$$

While not obvious in the above representation, it turns out that dx_1/dp takes on a sinusoidal form in t, which helps us locate its zeros quickly. To obtain this form, we first define

$$f_1(v, p) = \varepsilon\omega\pi^2 A \cosh(\pi^2 A p) \operatorname{sech}(\pi^2 A v) \times [\tanh(\pi^2 A p) - \tanh(\pi^2 A v)]$$

and

$$J(p) = \sqrt{\left(\int_p^\infty f_1(v, p) \cos(\omega v) \mathrm{d}v\right)^2 + \left(\int_p^\infty f_1(v, p) \sin(\omega v) \mathrm{d}v\right)^2}.$$

Then, after some trigonometric manipulations, it is possible to write

$$\frac{dx_1}{dp} = J(p)\cos[\omega(p-t)-\theta(p)],$$
$$\theta(p) = \cos^{-1}\left(\frac{\int_p^\infty f_1(v,p)\cos(\omega v)\mathrm{d}v}{J(p)}\right), \tag{D.1}$$

from which zeros can be obtained easily using a Newton–Raphson method. These represent parameter values p corresponding to fold points, as long as d^2x_1/dp^2 is sign definite. This takes the form

$$\begin{aligned}\frac{d^2x_1^s}{dp^2} &= \varepsilon\omega\pi^4A^2\cosh(\pi^2Ap)\\ &\quad\times\int_t^\infty \operatorname{sech}[\pi^2A(u-t+p)]\cos(\omega u)\\ &\quad\times\{2\tanh^2[\pi^2A(u-t+p)]\\ &\quad-\tanh[\pi^2Ap]\tanh[\pi^2A(u-t+p)]\\ &\quad-\tanh^2[\pi^2Ap]\}\mathrm{d}u+\varepsilon\omega\pi^4A^2\sinh(\pi^2Ap)\\ &\quad\times\int_t^\infty \operatorname{sech}[\pi^2A(u-t+p)]\\ &\quad\times\cos(\omega u)\{\tanh[\pi^2Ap]\\ &\quad-\tanh[\pi^2A(u-t+p)]\}\mathrm{d}u.\end{aligned} \tag{D.2}$$

It is straightforward to compute the p-derivatives of the x_2-coordinate in (4) to be

$$\frac{dx_2^s}{dp} = -\pi A\operatorname{sech}(\pi^2Ap),$$
$$\frac{d^2x_2^s}{dp^2} = \pi^3A^2\operatorname{sech}(\pi^2Ap)\tanh(\pi^2Ap). \tag{D.3}$$

Given expressions (D.1)–(D.3), the following geometrical quantities are easy to compute:

- The arclength between two points with parametric coordinates p_1 and p_2:

$$S(p_1,p_2) = \int_{p_1}^{p_2}\sqrt{\left(\frac{dx_1^s}{dp}\right)^2+\left(\frac{dx_2^s}{dp}\right)^2}\mathrm{d}p. \tag{D.4}$$

- The curvature at a general location p on the stable manifold:

$$\kappa(p) = \frac{\left|\frac{d^2x_2^s}{dp^2}\frac{dx_1^s}{dp}-\frac{d^2x_1^s}{dp^2}\frac{dx_2^s}{dp}\right|}{\left[\left(\frac{dx_1^s}{dp}\right)^2+\left(\frac{dx_2^s}{dp}\right)^2\right]^{3/2}}. \tag{D.5}$$

These expressions can also be used to determine the arclength and curvature of the *unstable* manifold, by substituting the expressions for $x_{1,2}^u$ instead.